*Journal of Ceramic Processing Research. Vol. 20, No. 4, pp. 424~430 (2019)*
*(Received 17 April 2019, Received in revised form 5 July 2019, Accepted 5 July 2019)*

J O U R N A L O F
**Ceramic Processing Research**

# Bone china figure fabrication using direct ink writing-type 3D printing technology

**Jung-Hoon Choi[a,b], Kyu-Hong Hwang[a], Ung-Soo Kim[b], Kuk-Hyeon Ryu[b], Kwang-Bo Shim[c], Seung-Min Kang[d] and Woo-Seok Cho[b,*]**

[a]*Department of Materials Science and Engineering, Gyeongsang National University, 501, Jinju-daero, Jinju-si, Gyeongsangnam-do, Korea*
[b]*Korea Institute of Ceramic Engineering and Technology, 3321 Gyeongchung-daero, Sindun-myeon, Icheon-si, Gyeonggi-do, Korea*
[c]*Department of Materials Science and Engineering, Hanyang University, Seoul 04763, Korea*
[d]*Department of Advanced Materials Science and Engineering, Hanseo University, Seosan, Korea*

**We carried out material and process optimization to fabricate a bone china figure using the direct ink writing-type 3D printing technology. To improve the viscoelastic properties of the bone china paste, we added PEG and glycerin and analyzed the rheological properties. The lowest viscosity was obtained when a mixture of 1 wt% PEG and 4 wt% glycerin was added to the paste, which resulted in excellent movement speed of the material in the system. A solvent content of 25% showed the best printing properties when water was used as the single solvent. In the ethanol-added solvent investigated to improve the shear yield strength, the best printing properties were observed for 40% ethanol. However, at an ethanol content of 50% or more, the drying rate increased excessively, and peeling and cracking between the layers were observed. The shell thickness was set as 4.8 mm or more considering that the thickness would be reduced in the post-treatment process. In the final bone china figure fabricated according to the aforementioned optimization, the concordance rate of the completed figure to the digital sketch was approximately 74% in the comparison including the surface curves, and 93% for the frame alone.**

**Key words: Direct Ink Writing, Bone China, Figure, 3D Printing.**

## Introduction

Bone china is superior to general ceramics in terms of flexural strength and chipping resistance. It has excellent whiteness, translucency, and brightness, and is used mainly for high-quality dinnerware and molding sculptures. Generally, the raw materials used for the fabrication of bone china bodies are mixed in the ratio of 50 wt% bone ash, 25 wt% clay, and 25 wt% feldspar. Quartz is partially added to reduce pyroplastic deformation. Compared with general ceramics, the clay ratio is low, which leads to low plasticity and a very narrow temperature range of heat treatment [1].

First, the product prototype and mold are fabricated, and then the bone china figures are formed by slip casting or pressure casting. Afterward, the final product is obtained by drying, glazing, and decoration [2]. Here, the application of 3D printing technology obviates the necessity of a pretreatment step for product molding, such as body form and mold fabrication, and addresses the limitations of fabrication arising from the complexity of the design. In addition, since it is based on a digital file, digital pre-verification technology can be used to evaluate the aesthetic and structural properties of the product, thereby reducing unnecessary trial and error [3, 4].

Direct ink writing-type (DIW) 3D printing technology is a method of extruding paste materials as filaments using an extruder [5-7]. During printing, the paste is transferred and extruded under an external stress from the feed tank in the form of a syringe through the physical screw to the fine nozzles. The resolution of the figure is governed by the diameter of the extruded filament. The thinner the filament diameter, the thinner is the deposited layer and the higher is the surface vertical resolution. To pass through the fine nozzles without breaking, the material must possess excellent plasticity and shear thinning behavior. In addition, it must dry quickly or have a high viscosity to resist deformation due to gravity and external stress after extrusion [8, 9].

In this study, to fabricate bone china figures using the DIW 3D printing technology, materials with optimized viscoelastic properties and improved shear yield strength were developed by extrusion. The bone china figures were fabricated using the optimized materials and its similarity with the digital sketch was analyzed to evaluate the molding quality. This process was divided into four steps: optimization of raw materials,

*Corresponding author:
Tel : +82-55-792-2630
Fax: +82-31-645-1440
E-mail: wscho@kicet.re.kr

evaluation of properties, molding and post-treatment, and sintering. In addition, we describe and discuss the points of consideration for DIW 3D printing.

## Experiments

The bone china material used in this experiment had a water content of 20% and was supplied by Korea Ceramics Co., Ltd. Polyethylene glycol (HS-BD20A, San Nopco Korea, Korea) (1% and 3%) and glycerin (Daejung, Korea) (2% and 4%) were added to optimize the viscoelastic properties of the bone china. The rheological properties of the paste were analyzed using a rotational rheometer (HAAKE MARS III, Thermo Fisher Scientific Inc., Germany).

To analyze the extrusion properties of the bone china paste, we simplified the feeding system of the DIW 3D printer, as shown in Fig. 1, and recorded the movement speed with time. The feed tank was filled with bone china paste and pressurized to 5.2 kgf/cm$^2$ to measure the time at which the material passes the points (marked at 100 mm intervals) shown in Fig. 1. Eight observation points were determined based on the 800 mm tube required for a smooth head movement range of a normal DIW-type 3D printer.

To determine the optimal solvent content of the bone china paste, we adjusted the distilled water content to 15, 20, 25, 30, and 35% of the solids. A specimen with dimensions of 15×15×50 mm$^3$ was printed (tilted bar printing test) at a tilt angle of 5° with the y-axis. The 3D printer used in the test was a Delta 2040 Clay (WASP 3D Printer, Italy) with an 800-μm-diameter nozzle. For smooth molding of the bone china paste, we reduced the initial layer print speed by 25% from 20 mm/min to 15 mm/min and lowered the general print speed from 50 mm/s to 27 mm/s. In addition, we increased the internal pressure of the material feed tank from the recommended 4.0 kgf/cm$^2$ to 5.2 kgf/cm$^2$, limited the length within 1000 mm from the material feed tank to the extrusion head, and suppressed the load that may occur during the feeding process. After drying the molded specimen, its 3D digital information was extracted using a 3D scanner (AICON PrimeScan R5, Hexagon, USA). We then quantitatively analyzed the malformation error by comparing the extracted digital information with the initial digital sketch. Fig. 2 is a schematic diagram of the process of acquiring the digital information after molding and comparing it with the initial digital sketch.

To minimize material deformation after extrusion, we replaced distilled water with ethanol, which has a higher evaporation rate and observed the changes. The bone china materials were prepared with different substitution ratios of ethanol (0, 20, 40, 60, 80, and 100%) and a tilted bar printing test was performed as before. The total solvent concentration was fixed as 35%.

We chose a digital sketch of a lion for printing to represent the complex surface curvature. We guided the printer to attain a structurally stable pose and selected a shape narrowing in the vertical direction to minimize deformation due to gravity during the sintering process. In addition, we reduced the overhang area to minimize unnecessary support assignment. Editing and extraction of the surface curvature was performed using Delcam's ArtCam software and pixologic's ZBrush.

A nozzle with a diameter of 800 μm was used for the DIW 3D printer, and the pressure of the material feed tank was set as 5.2 kgf/cm$^2$. Furthermore, to adhere the four initial layers to the stage, the layers were deposited first to a thickness of 0.2 mm and then 0.4 mm. The shell thickness was set as 4.0 mm considering that the thickness would reduce during post-treatment after molding. The internal square grating structure was set

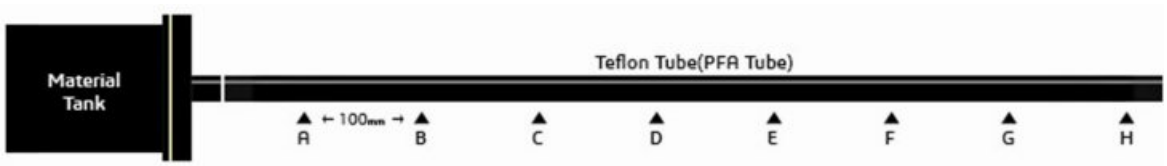


**Fig. 1.** Analytical equipment for determining material extrusion properties using DIW 3D printer material feed system.

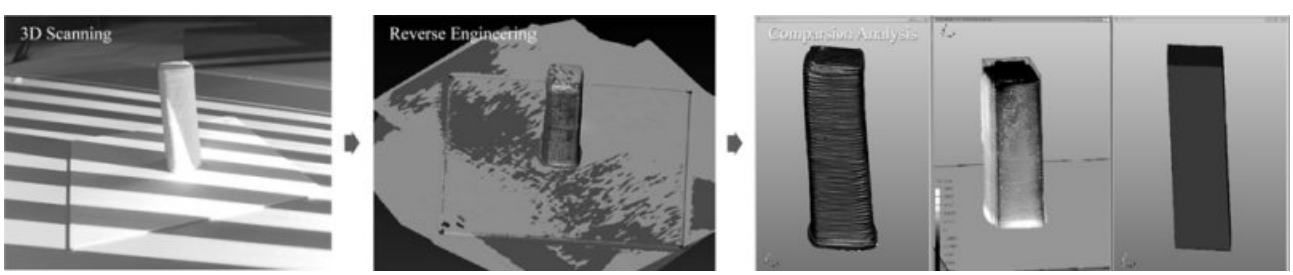


**Fig. 2.** Analysis of concordance rate between original digital sketch and molded figure.

so that the spacing between the gratings do not exceed 7 mm. After printing, the bone china figure was dried, sintered primarily at 1250 °C, and glazed. Finally, the product was sintered secondarily at 1000 °C to complete fabrication. To quantitatively analyze the accuracy of the completed figure, we extracted digital information using a 3D scanner (AICON PrimeScan R5, Hexagon, USA) and compared it with the original digital sketch. Delcam's PowerShape software was used to determine the concordance rate.

## Results and Discussion

We used two types of additives to optimize the viscoelasticity and extrusion properties of the bone china and analyzed its rheological properties (Fig. 3). When PEG was added, the change in viscosity of the bone china was insignificant. However, the viscosity greatly decreased when glycerin was added. The viscosity increased when 1% PEG was added to the sample, but decreased upon glycerin addition.

The decrease in viscosity with increasing shear rate indicates that fluidity is more easily attained when force is applied to the bone china paste. The slope of change in viscosity with shear rate shows that the shear thinning behavior of the bone china paste is larger when glycerin is added. For the bone china paste, as the solvent concentration is low, the addition of PEG having a high molecular weight induces the bridge effect between the raw material particles and increases the viscosity [10].

Fig. 4 shows the movement time of the bone china paste containing different additives through the DIW material feed system. The best extrusion properties were observed for the paste with 4 wt% glycerin. Generally, the extrusion speed increased with the addition of PEG. The mixture of PEG and glycerin exhibited the second-best result. The graph shows a large change due to the difference in additive. This is due to the important role of the viscoelastic properties of the material and the lubricity in the actual feed line, which must pass through the narrow, long pipe.

When the bone china paste is deposited using the DIW 3D printer, the forces applied to the height axis of the sculpture can be largely classified into gravity and stress that occur between the movements of the nozzle [11]. As the deposition process is repeated, the height and weight of the molding increase, thereby increasing the influence of gravity on the material and weakening the resistance of the nozzle to the movement stress. Therefore, if the shear yield stress of the bone china paste is larger than the gravity, then deformation during printing can be lowered.

Fig. 5 shows the shear modulus (G' and G") of the sample containing 4 wt% glycerin. The linear viscoelastic range is the range in which the internal structure of the

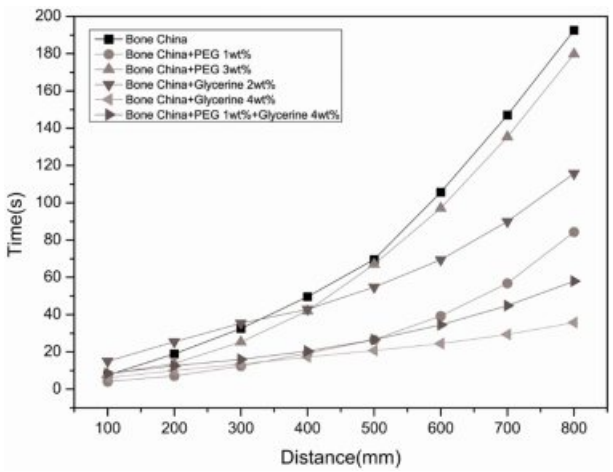


**Fig. 4.** Extrusion speed of bone chain paste containing different additives.

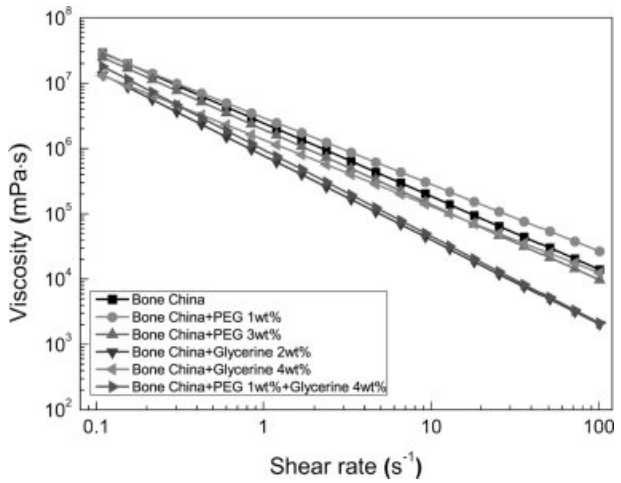


**Fig. 3.** Change in viscosity of bone china paste containing different additives.

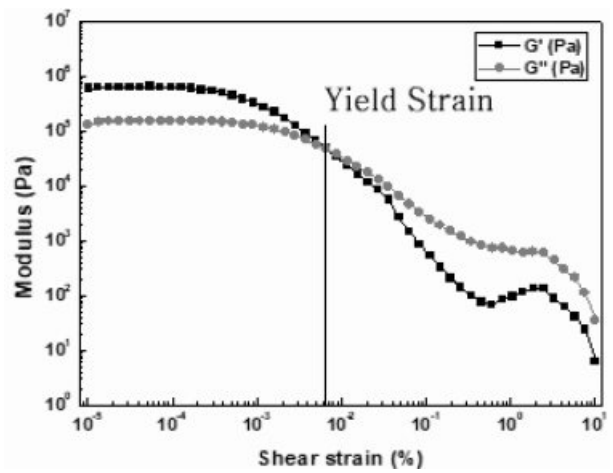


**Fig. 5.** Shear modulus of sample containing 4 wt% glycerin.

**Table 1.** Shear yield strength according to type and content of binder.

| Category | PEG 1 wt% | PEG 3 wt% | Glycerin 2 wt% | Glycerin 4 wt% | PEG 1 wt% + Glycerin 4 wt% |
|---|---|---|---|---|---|
| Yield strain (%) | 0.0156 | 0.0207 | 0.0118 | 0.0067 | 0.0156 |

sample is not destroyed; if G' > G" then the sample behaves like a solid, and its value can represent the stiffness of the sample [12]. The intersection of G' and G" is the point at which the internal structure of the sample breaks and deforms, which is the shear yield strength. Table 1 summarizes the yield strain depending on the additives. It is noteworthy that when a mixture of PEG and glycerin is added, the viscosity is low, but the shear yield strength is relatively high. Under this condition, the bone china paste easily attains flowability when force is applied and is resistant to changes due to external stress after deposition.

We conducted a solvent optimization experiment for bone china with 1% PEG and 4 wt% glycerin, which shows the best viscoelasticity and extrusion properties. Distilled water was added at 15, 20, 25, 30, and 35 wt% with respect to the bone china solid to prepare a paste, and then the specimen was printed.

Fig. 6 is a photograph obtained as a digital file by reverse engineering the printing results according to the ratio of distilled water. In the 15 wt% solvent sample, due to the low water content, adhesion between the layers was not achieved from the beginning of molding and was continuously pushed in the direction of nozzle movement. Unstable deposition behavior continued, and molding eventually failed due to collapse in the seventh layer. The concordance rate obtained by calculating only the initial seven layers with respect to the original was found to be 3.45%.

The 20 wt% solvent sample showed a better deposition behavior but still had a low bond strength between the layers. Each of the approximately 8th to 12th layers showed a phenomenon in which the accumulated stress due to nozzle movement peeled the region at which the bond between the layers was relatively low. Though we observed a concordance rate of approximately 23.06%, we determined that the data of the central part, which was peeled relatively intact, was reflected.

Excellent adhesion between the layers was observed in the 25 wt% solvent sample. In addition, with a sufficient amount of solvent, no breakage was observed for the paste extruded from the nozzle. We also found that the paste resisted the stress generated in the moving direction of the nozzle. The concordance rate of the finished specimen was calculated to be more than 95%, which indicated that the model of the digital sketch is almost perfectly reflected when the surface curvature generated between the layers is considered.

The 30 wt% solvent specimen initially facilitated a normal printing process; however, excessive solvent accumulated continuously inside the extruder of the DIW 3D printer. The accumulated moisture fell onto the sculpture along the nozzle, and the accumulated moisture made the bone china paste in the form of slurry at the end of printing. The calculated concordance rate was relatively high at 78%; however, printing was determined impossible due to the accumulated moisture.

The 35 wt% solvent sample showed a very low shear yield strength of the bone china paste due to the presence of excessive solvent. After approximately 50% printing, the figure tilted to one side by 12° under its own weight. After the completion of printing, it could not withstand its own weight and collapsed

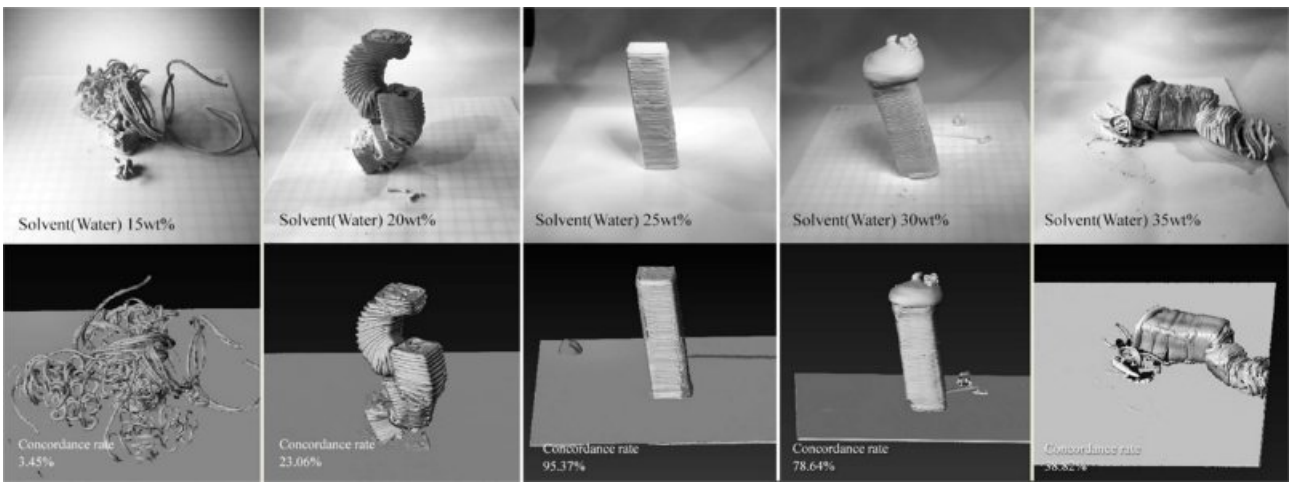


**Fig. 6.** 3D printing molding results and 3D scanning data of molding according to solvent content.

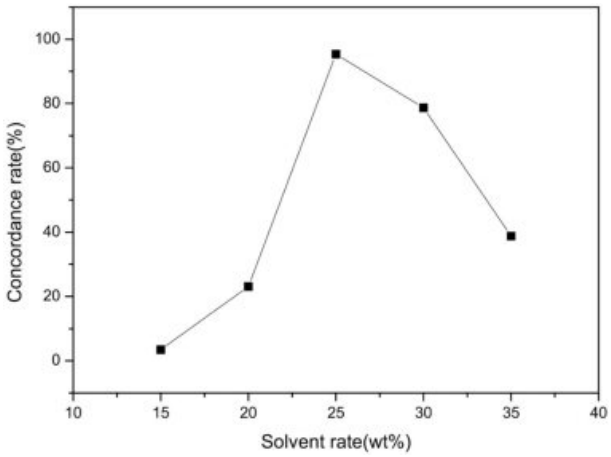


**Fig. 7.** Change in concordance rate of original digital sketch according to solvent content.

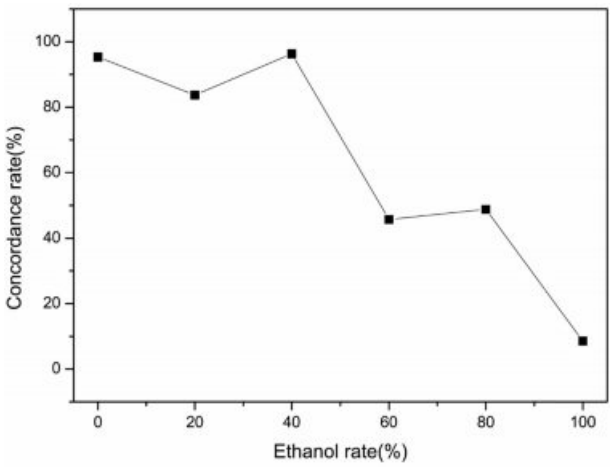


**Fig. 9.** Change in concordance rate of original digital sketch according to ethanol content.

before being sufficiently dried. The concordance rate was approximately 38%. The graph of concordance rate as a function of solvent content shows that the best printing properties were obtained at 25% solvent content (Fig. 7).

To increase the hardening speed after extrusion of the 25 wt% solvent sample, distilled water was replaced with ethanol and a tilted bar printing test was conducted. Fig. 8 shows the concordance rate between the printing results and the digital sketch according to the ethanol content. As can be seen, the 0~20 wt% solvent specimen with a low ethanol content exhibited slanting or layer bending during the printing process. This is because the shear yield strength of the deposited sculpture is lower than the nozzle stress and gravity.

The drying speed was notably fast for an ethanol content of 40% or more. For an ethanol content of nearly 60%, the adhesion between the layers decreased and peeling occurred due to a faster drying rate than necessary. Visible defects were observed at 80% or more ethanol content, and at 100%, the figure peeled from the tray and collapsed during the printing process. Fig. 9 shows the concordance rate between the printing result and the original digital sketch according to the ethanol content.

To prevent unnecessary material filling during the printing process, the outer area of the digital sketch was set as Shell and the remaining area was set as Core. Fig. 10 shows the photograph of a printing cross-section of the shell and core. The thickness of the shell was set as four line widths (4.8 mm) considering that the partial thickness would be reduced during post-treatment of the bone china figure molding process. The internal structure spacing was set as 9 mm, a size at which the cap layer does not collapse, considering the viscoelastic properties of the bone china paste. In the post-treatment process in which the uneven cross-section caused by deposition is removed, when the water content of the figure decreased to approximately 15%, the wetted brush was moved in the vertical direction of the layer to remove the irregularities.

We used the bone china paste optimized through the above experiments for fabricating a bone china figure. Fig. 11 shows the level of similarity between the completed bone china figure and the digital sketch. On

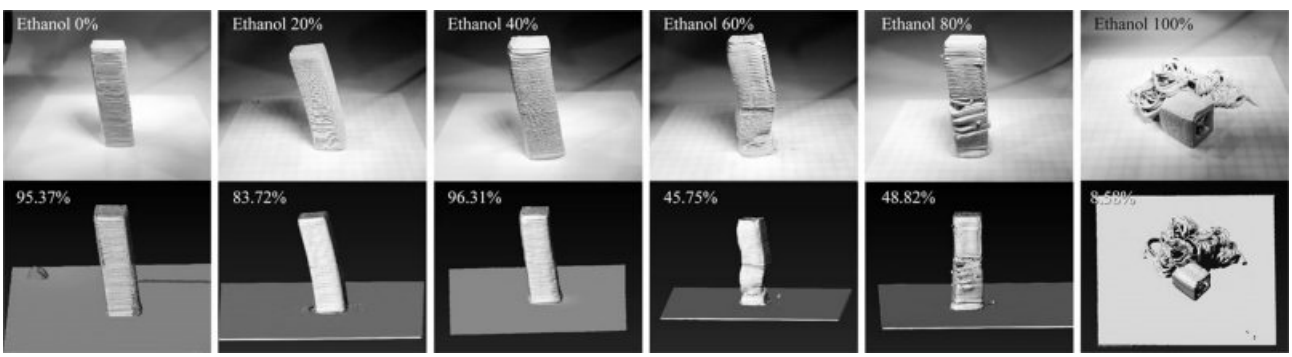


**Fig. 8.** 3D printing molding results and 3D scanning data according to ethanol content.

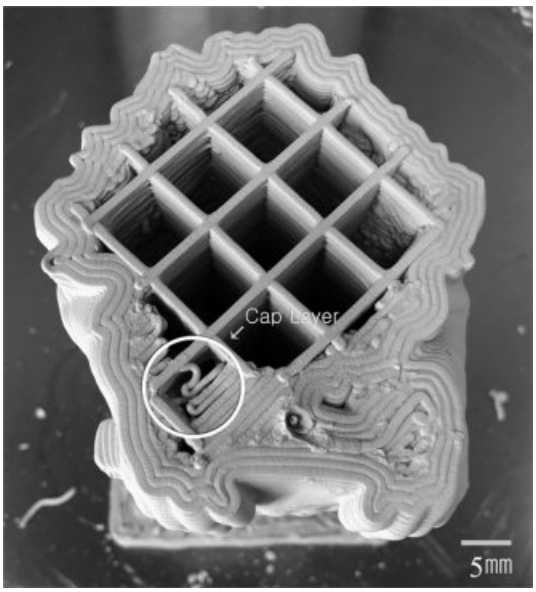


**Fig. 10.** Shell/core cross section.

comparison, a concordance rate of approximately 93% was observed for the curves with the surface resolution excluded, and approximately 74% concordance rate was observed when surface curve shapes were added. The concordance rate decreased in the latter case possibly due to the surface smoothness caused by the post-treatment process and the reduction in surface resolution due to the glaze. Fig. 11(a) shows that the discordance area mainly appeared at the ends of the curves, and Fig. 11(b) shows a photograph of the finished bone china figure. The figure proves that printing was successful with excellent surface resolution.

## Conclusions

We carried out material and process optimization for fabricating a bone china figure using the DIW 3D printing technology. To improve the viscoelastic properties of the bone china paste, we added PEG and glycerin, and analyzed the rheological properties. While the addition of PEG caused an insignificant change in viscosity, the viscosity decreased greatly with the addition of glycerin. Furthermore, we observed large changes in the extrusion time according to the type of additive used. This is because of the important role of the viscoelastic properties of the material and the lubricity in the actual feed line, which must pass through the narrow, long pipe. In terms of material feed speed, the best extrusion properties were observed for a mixture of 1 wt% PEG and 4 wt% glycerin.

The investigation of optimal solvent content of the bone china paste revealed that the 25 wt% solvent sample possessed excellent adhesion between the layers. In addition, with a sufficient amount of solvent, no breakage of the paste extruded from the nozzle was observed. We also found that the paste resisted the stress generated in the moving direction of the nozzle. The concordance rate of the finished specimen exceeded 95%, which indicated that the model of the digital sketch is almost perfectly reflected.

Further, the amount of ethanol added to improve the shear yield strength after extrusion was optimized. It

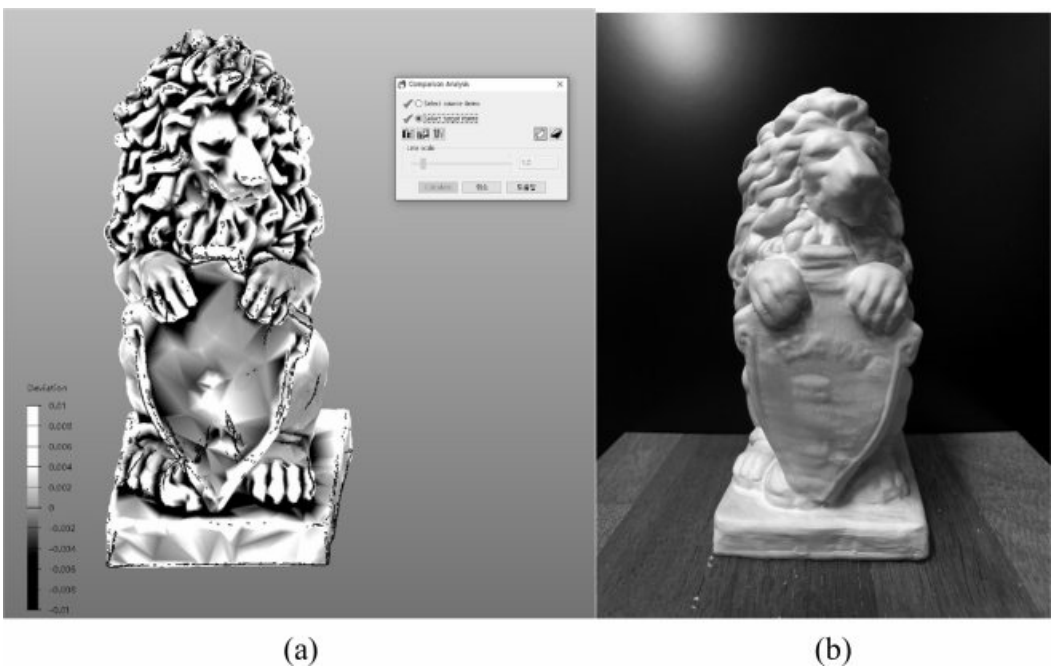


**Fig. 11.** Comparison analysis surface plot (a) and finished bone china figure (b).

was found that the addition of 40% ethanol resulted in the highest printing quality. Moreover, as the amount of ethanol increased, the drying speed as well as the resistance to gravity and external stress increased. However, at an ethanol content of 50% or more, the drying rate increased excessively, and peeling and cracking between the layers were observed.

We applied the optimized bone china paste to fabricate a bone china figure. The thickness of the shell was set as four line widths (4.8 mm) considering that the partial thickness would be reduced in the post-treatment step of the bone china figure molding process. The print speed was set as 27 mm/s considering the viscoelastic properties of the bone china paste, and the spacing of the internal structure was set as 9 mm. For surface post-treatment, when the water content of the figure decreased to approximately 15%, the wetted brush was moved in the vertical direction of the layer to remove the irregularities.

The bone china figure fabricated thereof showed a concordance rate of approximately 74% between the finished figure and the digital sketch with surface curves included, and a concordance rate of approximately 93% for the frame alone.

## Acknowledgement

This work was supported by the Technology Innovation Program (10070165, Convergence of Traditional Ceramicware Process and Digital 3D Printing Process for High-Value-Added Bone China Porcelain) funded by the Ministry of Trade, Industry & Energy (MOTIE, Korea).

## References

1. F. H. Norton, in “Fine Ceramics Technology and Applications” (McGraw-Hill, Inc. 1970) p. 346-355.
2. Y. Zhang, N. Zhou, W. Li, J. Li, S. Nian, X. Li, and J. Sui, Ceram. Int. 42[13] (2016) 14910-14927.
3. J.H. Choi, E.T. Kang, J.W. Lee, U.S. Kim, and W.S. Cho, J. Ceram. Process. Res. 19[1] (2018) 43-49.
4. H. Kwon, S. Bukkapatnam, B. Khoshnevis, and J. Saito, Rapid Prototyp. J. 3[3] (2002) 147-160.
5. J.H. Lee, H.J. Hwang, J.H. Kim, K.T. Hwang, K.S. Han, Korean J. Mater. Res. 28[2] (2018) 95-100.
6. I. Grida and J. R. G. Evans, J. Eur. Ceram. Soc. 23[5] (2003) 629-635.
7. Z. Fu, M. Freihart, L. Wahl, T. Fey, P. Greil, and N. Travitzky, J. Eur. Ceram. Soc. 37[9] (2017) 3115-3124.
8. A. M’Barki, L. Bocquet, and A. Stevenson, Sci. Rep. 7 (2017) 1-10.
9. S. Ketel, G. Falzone, B. Wang, N. Washburn, and G. Sant, Cement Concrete Comp., In Press (2018) p. 14.
10. Y. Fukuda, T. Togahi, Y. Suzuki, M. Naito, H. Kamiya, Chem. Eng. Sci. 56[9] (2001) 3005-3010.
11. J. A. Lewis, Curr. Opin. Solid St. M. 6[3] (2002) 245-250.
12. M. R. Somalu and N. P. Brandon, J. Am. Ceram. Soc. 95[4] (2012) 1220-1228.